IOP Publishing Phys. Med. Biol. 66 (2021) 145011 https://doi.org/10.1088/1361-6560/ac1023

Physics in Medicine & Biology

IPEM Institute of Physics and Engineering in Medicine



RECEIVED
30 March 2021

REVISED
23 June 2021

ACCEPTED FOR PUBLICATION
30 June 2021

PUBLISHED
14 July 2021

PAPER

# The quantification of liver fat from wave speed and attenuation

K J Parker and J Ormachea

Department of Electrical and Computer Engineering, University of Rochester, 724 Computer Studies Building, Box 270231, Rochester, NY 14627, United States of America

E-mail: kevin.parker@rochester.edu

Keywords: steatosis, fatty liver, quantitative estimates, elastography, ultrasound, staging

## Abstract

A framework is developed for estimating the volume fraction of fat in steatotic livers from viscoelastic measures of shear wave speed and attenuation. These measures are emerging on clinical ultrasound systems' elastography options so this approach can become widely available for assessing and monitoring steatosis. The framework assumes a distribution of fat vesicles as spherical inhomogeneities within the liver and uses a composite rheological model (Christensen 1969 *J. Mech. Phys. Solids* **17** 23–41) to determine the shear modulus as a function of increasing volume of fat within the liver. We show that accurate measurements of shear wave speed and attenuation provide the necessary and sufficient information to solve for the unknown fat volume and the underlying liver stiffness. Extension of the framework to compression wave measurements is also possible. Data from viscoelastic phantoms, human liver studies, and steatotic animal livers are shown to provide reasonable estimates of the volume fraction of fat.

## 1. Introduction

The noninvasive quantification of fat content in the liver is a longstanding goal with major clinical significance. Non-alcoholic fatty liver disease is the most prevalent chronic liver disease, affecting approximately 25% of the global population (Younossi *et al* 2016, Nasr *et al* 2020), however options for measuring and monitoring the progression of steatosis have been limited. To address this need, there are a number of efforts to quantify steatosis using different imaging modalities (Cowin *et al* 2008, Xia *et al* 2012, Lee and Park 2014, Kramer *et al* 2017, Zhang *et al* 2018, Ferraioli 2019, Starekova and Reeder 2020).

Ultrasound has potential for the study of steatosis in livers (Romero-Gómez and Cortez-Pinto 2017, Ferraioli *et al* 2019, Lin *et al* 2019, Nguyen *et al* 2019, Jesper *et al* 2020, Pirmoazen *et al* 2020, Tamura *et al* 2020). Following the categories outlined in Pirmoazen *et al* (2020), ultrasound assessments of steatosis have utilized a number of approaches, including ultrasound attenuation measures, backscatter measures, comparative hepato-renal measures, envelope statistics, speed of sound, and elastography measures. A full description of them with detailed references are found in Pirmoazen *et al* (2020), however none of these approaches are currently in widespread clinical use, and many studies still rely on biopsy or MRI techniques for a reference standard measurement. Furthermore, the presence of simultaneous medical conditions that also influence these parameters as co-factors complicates their interpretation (Barr *et al* 2015, Poul and Parker 2021). For these reasons, the goal of obtaining accurate measures of liver steatosis from ultrasound imaging systems remains a compelling objective.

To address this clinical goal, we derive a method for absolute quantitative estimates of the volume fraction $V$ of liver fat, assuming the liver can be modeled as a composite medium with inclusions comprised of viscous fat in vacuoles. The composite model formulation introduced by Christensen (1969) for spherical inclusions is employed to quantify the effects of fat vacuoles accumulating in steatotic livers.

## 2. Theory

### 2.1. General approach

Our approach is to analyze the complex (real and imaginary, or elastic and lossy) nature of the liver's viscoelastic properties as increasing amounts of fat are incorporated within the liver in the form of spherical vesicles. The inhomogeneous, steatotic liver is treated as a composite material with baseline properties related to the normal lean liver plus increasing loss terms as fat volume fraction $V$ increases. The theory of the elastic modulus of a composite material comprised of spherical inclusions was derived in a landmark paper by Christensen (1969). The principle of minimum strain energy was applied in a deformed elastic medium with inhomogeneities comprised of spherical inclusions. Upper and lower bounds on the strain energy were obtained beginning with volume integral formulations of strain energy in deformed media. Simplifications for the effective shear modulus were found for the limiting cases of the volume fraction $V$ of spheres being small, more generally $V < 0.5$, in the form of equation (16) of Christensen (1969). A more recent treatment of different forms of composites and other inclusion shapes can be found in chapter 9 of Lakes (1999b). We employ the most relevant solution, the low concentration case for small volume fraction $V$ of fat (triglyceride-filled spherical vacuoles) with complex shear modulus $G_2(\omega)$, contained within a viscoelastic liver matrix modeled as $G_1(\omega)$, and where $\omega$ is the shear wave radial frequency. Given $G_2(\omega)$, $G_1(\omega)$, and $V$, the new composite liver representing simple steatosis will have a shear modulus $G_c(\omega)$ given by:

$$\frac{G_c}{G_1} = 1 - \frac{15(1-\nu_1)\left(1-\frac{G_2}{G_1}\right)V}{7-5\nu_1+2(4-5\nu_1)\frac{G_2}{G_1}}. \tag{1}$$

Assuming the liver's Poisson's ratio $\nu_1 \approx 0.5$, nearing the incompressible limit (Fung 1981), and writing the frequency dependence explicitly:

$$G_c(\omega) \approx G_1(\omega) - \frac{\frac{15}{2}[G_1(\omega)-G_2(\omega)]V}{\frac{9}{2}+3\left[\frac{G_2(\omega)}{G_1(\omega)}\right]}. \tag{2}$$

Let us assume a generalized power law behavior for normal liver, consistent with the Kelvin–Voigt fractional derivative model with the parallel elastic element $E_0$ near zero (Zhang *et al* 2007) and also consistent with the two-parameter microchannel flow model (Parker 2014, 2015). Thus, for normal liver, we generally assume that:

$$G_1(\omega) = G_0(i\omega)^a = G_0 \cdot \omega^a\left[\cos\left(\frac{a\pi}{2}\right) + i\,\sin\left(\frac{a\pi}{2}\right)\right], \tag{3}$$

where $G_0$ is a constant, $i$ is the imaginary unit $\sqrt{-1}$, and $a$ is the power law parameter. Furthermore, we assume a purely viscous fluid model for the fat within the spherical vacuoles:

$$G_2(\omega) = \eta \cdot i\omega, \tag{4}$$

where $\eta$ is the viscosity of the fat (Parker *et al* 2018a). In that case, the composite has a dramatic change in frequency response of $|G_c(\omega)|$, a function of the frequency and volume fraction $V$, since the contribution from the fat has no real elastic part and is purely imaginary. Once $G_c(\omega)$ is specified, the storage modulus and loss modulus can be plotted from the real and imaginary parts of $G_c(\omega)$, respectively. In addition, the complex wavenumber $\hat{k}$ is specified (Blackstock 2000, Carstensen and Parker 2014) as:

$$\hat{k} = \frac{\omega}{\sqrt{\frac{G_c(\omega)}{\rho}}} = \beta - i\alpha = \frac{\omega}{c_p} - i\alpha, \tag{5}$$

where $c_p$ is the phase velocity, $\alpha$ is the attenuation, $\rho$ is the mass density (assumed to be approximately 1 g cm$^{-3}$ for soft tissues), and $\beta$ is the real part of the wavenumber. Phase velocity and attenuation are functions of frequency and can be measured experimentally using clinical imaging platforms with appropriate elastography options (Sharma *et al* 2019). Assuming $c_p$ and $\alpha$ have been measured accurately, we can determine $G_c(\omega)$ as:

$$G_c(\omega) = \frac{\rho\omega^2}{\left(\frac{\omega}{c_p} - i\alpha\right)^2}. \tag{6}$$

To address the inverse problem, we now ask how $V$ can be determined experimentally. Let us assume that the parameters in equation (4) are known for the fat vesicles, that both frequency and viscosity are known, and that $G_c(\omega)$ is also known from experimental measurements as in equation (6). Rewriting equation (2) we have:

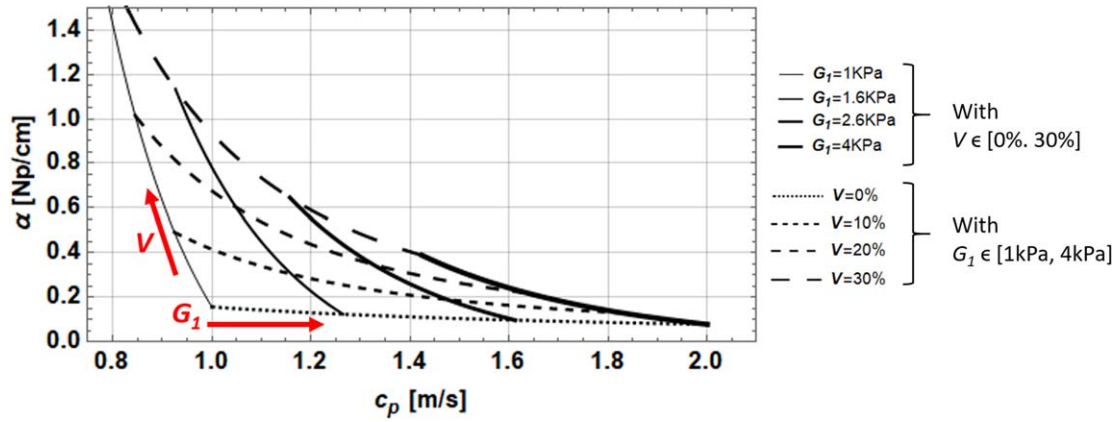


**Figure 1.** Nomogram providing graphical estimates of fat volume fraction $V$ and liver matrix shear modulus $G_1$, given measurements of shear wave attenuation (vertical axis) and shear wave speed (horizontal axis) and assuming a shear wave frequency of 100 Hz. The two-dimensional parametric space is illustrated with particular values of $V$ from 0% to 30% (dashed lines), and also for particular increasing values of $G_1$, (solid lines). Any measured liver values of attenuation and speed can be plotted on the nomogram to provide a graphical estimate of the $V$ and $G_1$ values for that liver.

$$G_c(\omega) = G_1(\omega) + \frac{5G_1[-G_1(\omega) + G_2(\omega)]V}{3G_1(\omega) + 2G_2(\omega)}. \tag{7}$$

This is actually two equations, one for the real part and one for the imaginary part. To see this in a more simple fashion, we initially consider a special case where $G_2$ is purely imaginary (fat) and $G_1$ is purely real (elastic liver). So in that special case, the real part of the composite $\mathrm{Re}\,[G_c]$ and the imaginary part $\mathrm{Im}[G_c]$ can be clearly separated:

$$\mathrm{Re}\,[G_c] = G_1 + \frac{5G_1(-3G_1^2 + 2\boldsymbol{G}_2^2)V}{9G_1^2 + 4\boldsymbol{G}_2^2}$$
$$\mathrm{Im}[G_c] = \frac{25G_1^2\boldsymbol{G}_2V}{9G_1^2 + 4\boldsymbol{G}_2^2} \tag{8}$$

and where in equation (8), $\boldsymbol{G}_2 = \eta\omega$, a magnitude term. In this example, assuming $G_c$ is known accurately from measurements and equation (6), we then have two equations in two unknowns, $G_1$ (liver) and $V$ (fat volume). The equations are cubic in $G_1$ and linear in $V$, and in principle these can be solved exactly, however random errors in measurements or parameters will invalidate the system of equations, so numerical methods that are regularized are preferred.

Taking the real and imaginary parts of equation (6) numerically gives two values for equation (8), which can be solved numerically for $G_1$ and $V$. This value of $V$ is an upper limit because equation (8) assumes all the loss is with the fat and the liver is purely elastic. Numerical solution routines are capable of finding the solution, or the global minimum of a corresponding minimization formulation. So the steps for quantifying liver fat volume fraction are:

- Measure $c_p$ and $\alpha$.
- Find the real and imaginary parts of the right-hand side of equation (6).
- Substitute those into the equation (8) for $\mathrm{Re}\,[G_c]$ and $\mathrm{Im}[G_c]$ with $\boldsymbol{G}_2 = \eta \times \omega$.
- Solve numerically for $G_1$ and $V$.

To be more realistic, a small imaginary term to $G_1$ (the liver shear modulus) can be included to approximate some baseline viscoelastic loss of normal liver. The resulting equations are more complicated than equation (8), but still are resolvable into real and imaginary parts, and are derived in appendix A. Unfortunately, that model introduces a third unknown variable, the relatively small, imaginary part of the normal liver. However *a priori* estimates can be employed. Alternatively assuming a small loss tangent (Lakes 1999b), the imaginary part of the shear modulus of liver can be set at some small fraction or percent of the real shear modulus. The governing equations incorporating a small imaginary component in the rheological model of the liver (exclusive of fat vacuoles) are given in appendix A.

### 2.2. Solution by nomogram

For a simplified approach, it is possible to employ an approximate graphical solution, or nomogram. In this strategy the forward problem is calculated from equations (4)–(7), and the resulting theoretical values of $\alpha$ and $c_p$ are plotted on a two-dimensional graph as a function of $\{V,\ G_1\}$ contours. In practical use, any pair of $\{\alpha, c_p\}$ measured from a patient is then located at a point on the graph which provides an immediate graphical estimate of the corresponding $\{V,\ G_1\}$ that are likely given the measured quantities. As an example, see figure 1. Note that as $c_p$ becomes larger than 1.5 m s$^{-1}$, the contours of constant $V$ begin to converge, meaning small errors in $\alpha$ estimates will result in large errors in determining $V$. Also, there are combinations of $\{\alpha,\ c_p\}$ that are not possible within the assumptions of the model. Patient data falling outside of the ranges shown would indicate that there were errors in the measurements or that the assumed model parameters, such as viscosity in equation (4), are incorrect and need to be adjusted.

## 3. Methods

Human livers and phantoms were scanned according to the protocols given in Parker *et al* (2018b) and Sharma *et al* (2019). The human subjects in Sharma *et al* (2019) were scanned under the requirements of informed consent and approval from the University of Rochester Research Subjects Review Board. The numerical solution was implemented using a minimization procedure in Mathematica (Version 12.1.1.0, Wolfram Research, Champaign, IL, USA) and choosing the internal simulated annealing method to avoid entrapment in local minima. The minimization approach simply subtracts the magnitude of the terms of equation (8), which should approach zero as the correct values of $V$ and $G_1$ are determined. The real and imaginary parts are equally weighted. The search parameter space is also limited within realistic ranges, and simulated annealing is utilized to avoid local minima. In that sense, the specific routine to find the minimum $T$ is as follows:

$$\begin{aligned}
&\underline{\text{Min}}\\
&\quad T = |\text{Re}\,[G_m{}'] - \text{Re}\,[G_c]| + |\text{Im}[G_m{}'] - \text{Im}[G_c]|\\
&\underline{\text{s.t.}}\\
&\quad 0.001 \quad < \quad V \quad < \quad 0.45\\
&\quad 700\ \text{Pa} \quad < \quad \text{Re}\,[G_1] \quad < \quad 12{,}000\ \text{Pa}\\
&\quad 0.90\,\text{Re}\,[G_m] \quad < \quad \text{Re}\,[G_m{}'] \quad < \quad 1.10\,\text{Re}\,[G_m]\\
&\quad 0.95\,\text{Im}[G_m] \quad < \quad \text{Im}[G_m{}'] \quad < \quad 1.05\,\text{Im}[G_m]
\end{aligned} \tag{9}$$

where $G_m$ is derived from the measured $c_p$ and $\alpha$ in equation (6), and where $G'_m$ is the approximate composite modulus entered into the equation, allowed to have a few percent variation from the measured modulus $G_m$ (due to the imprecision of measurements), and where the two unknowns are $G_1$ (the real part of the shear modulus of the liver) and $V$ (the volume fraction of fat vesicles) which are linked to $G_c$ by the equations in appendix A. The simulated annealing search algorithm searches under constraints on the permitted values of $V$ and $G_1$: $0.001 < V < 0.45$ and $700\ \text{Pa} < \text{Re}[G_1] < 12{,}000$ Pa. In order to match the data from Parker *et al* (2018b) and Sharma *et al* (2019), we assumed a frequency of 100 Hz for shear waves and a viscosity of 0.12 Pa-s for oil in phantoms and 0.4 for fat vesicles in liver. Using the 'NMinimize' function in Mathematica, the return of the global minimum is obtained from the expression:

$$\textbf{NMinimize}\left[\begin{matrix}\{T,\ \text{constraints}\},\ \{V,\ G_1,\ \text{Re}\,[G'_m],\ \text{Im}[G'_m]\},\\ \textbf{Method} \rightarrow \text{'Simulated Annealing'}\end{matrix}\right]. \tag{10}$$

In addition, the Spearman's rank correlation coefficient was used as a non-parametric measure of rank correlation, and the analysis of variance (ANOVA) was applied to determine if the $V$ results from the different steatotic scores have a common mean. The ANOVA test was performed after confirming that the estimated data follows a normal distribution, by applying a Shapiro–Wilk test and a quantile-quantile plot. Then, a multiple comparison test was performed, using the Bonferroni method, to determine the significance of differences between multiple groups means. The Shapiro–Wilk test was implemented by Öner and Kocakoç (2017). Other statistical tests were implemented using the Statistics and Machine Learning Toolbox in MATLAB (The MathWorks, Inc., Natick, MA, USA).

## 4. Results

The derived values, from the composite material model, of the real and imaginary parts of the shear modulus for the oil-in-gelatin phantoms are given in table 1. Note the general trend with increasing amounts of oil in the form of spherical inclusions is to decrease (soften) the real modulus, and also to decrease the imaginary

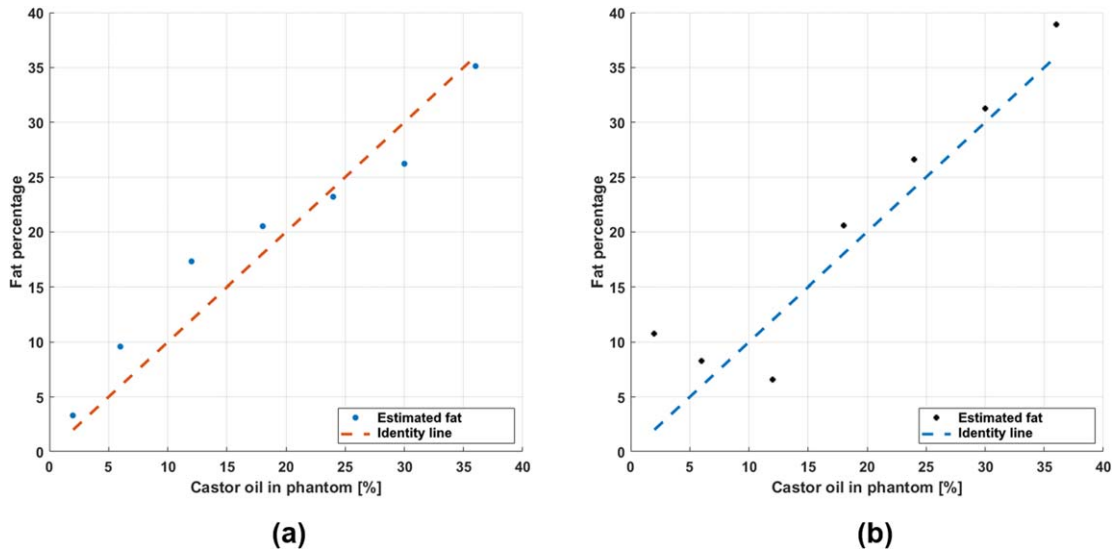


**Figure 2.** Numerical solution of volume percentage of fat in the gelatin-based phantoms with different amounts of castor oil percentages used in Parker *et al* (2018a). (a) $V$ estimates using the complex shear modulus values from table 1 and (b) $V$ estimates using the median complex shear modulus when using the median results of shear wave speed and shear attenuation from figures 9 and 10 of Parker *et al* (2018a). The red or blue dash lines represents a perfect correlation between the applied oil volume percentage in the phantoms and the $V$ estimates.

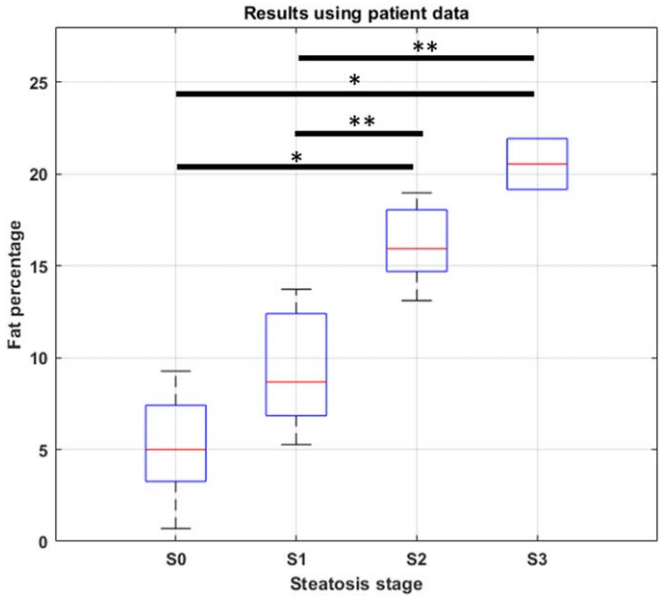


**Figure 3.** Numerical solution of volume percentage fat in 20 patients scanned in Sharma *et al* (2019). The steady increase in estimated $V$ is observed and confirmed by a Spearman's rank correlation coefficient equal to 0.88. The ANOVA ($p$-value of 2.96e-06) and the multi-comparison tests show that there is a significant difference between groups S0 and S2, S0 and S3, S1 and S2, and S1 and S3. $^{*}p < 0.01, ^{**}p < 0.05$.

**Table 1.** Shear moduli of oil-in-gelatin phantoms.

| Oil percent | $c_p$ (m s$^{-1}$ at 100 Hz) | $\alpha$ (Np m$^{-1}$ at 100 Hz) | Complex shear modulus $G$ (Pa) |
|---|---|---|---|
| 2% | 2.13 | 5.91 | 4539.02 + 182.18i |
| 6% | 2.05 | 6.41 | 4226.06 + 177.55i |
| 12% | 1.94 | 7.35 | 3756.63 + 170.62i |
| 18% | 1.81 | 8.61 | 3287.19 + 163.69i |
| 24% | 1.68 | 10.39 | 2817.75 + 156.75i |
| 30% | 1.53 | 13.05 | 2348.31 + 149.81i |
| 36% | 1.37 | 17.37 | 1878.88 + 142.88i |

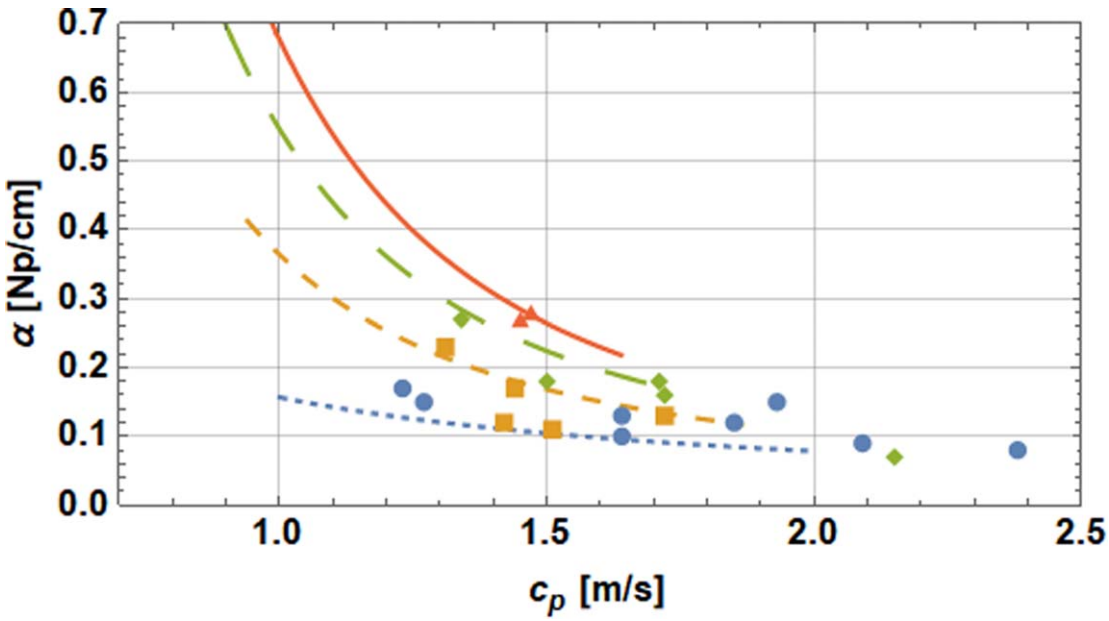


**Figure 4.** Theory versus experiments, viscosity $=$ 0.4 Pa s for fat, showing patients with steatosis scores of S0 (blue circles), S1 (yellow squares), S2 (green diamonds), and S3 (red triangles). Theoretical curves represent values of $V$ equal to 0% (blue), 8% (yellow), 15% (green), and 20% (red) covering different liver shear modulus values, $G_1$, between 1 and 4 kPa. The patient data are found to be stratified such that the two cases of S3 are located near the $V = 20\%$ curve. The cases of S2 are located near the $V = 15\%$ curve, with cases of lower grade steatosis below these.

modulus, however we note that this effect is strongly dependent on the frequency through equation (4) and so would require re-evaluation for other shear wave frequencies.

Figure 2 shows the results for the simulated annealing algorithm determining the volume fraction of fat in the phantoms. The numerical minimization search procedure was run on the oil-in-gelatin phantom series of experiments. Figure 2(a) shows the numerical results using the complex shear modulus values from table 1, and figure 2(b) shows the numerical results using the median complex shear modulus when using the median results of shear wave speed and shear attenuation from figures 9 and 10 of Parker *et al* (2018a).

Figure 3 shows the numerical estimates from 20 patients within the Sharma *et al* study (2019), showing the estimated volume percentage $V$ of fat as a function of biopsy results scored for steatosis stages S0–S3. The middle of the elastography region of interest (ROI) was placed between 3 and 6 cm deep and at least 1–2 cm below the capsule. Ten repeat elastography scans' ROIs were obtained near or in the sample plane of the biopsy. The steady increase in estimated $V$ is observed. Then Spearman's rank correlation coefficient was 0.88 with $p$-value equal to 2.65e-07. The applied Shapiro–Wilk test ($p$-value equal to 0.49) and a quantile-quantile plot (which produces an approximately straight line) confirmed that the estimated data follows a normal distribution. For the ANOVA test, the within-groups and between-groups degrees of freedom were 16 and 3, respectively. A $F$-statistic of 24.79 was obtained and the $p$-value of 2.96e-06 indicates that estimated volume fraction $V$ of fat values from the different steatosis groups are not the same. The $p$-values for the multiple comparison test show that there is a significant difference between groups S0 and S2 ($p = 2.45\text{e-}05$) and S3 ($p = 2.30\text{e-}05$). The same is true for groups S1 and S2 ($p = 0.0096$) and S3 ($p = 0.0014$). However, there was no significant difference between groups S0 and S1 ($p = 0.1122$), and between S2 and S3 ($p = 0.5134$).

Figure 4 provides the individual patient data from Sharma *et al* (2019) plotted on the nomograph. Curves show discrete values of fat volume fraction $V$ at increasing values, and generally correspond to increasing grades of steatosis.

## 5. Discussion

The results in phantoms and human livers show reasonable agreement of our quantitative solutions against independent measures of fat, however limitations of this method include the uncertainties in measurements of $\alpha$ and $c_p$, within clinical systems. The variability between systems and within patients' abdominal structures are a subject of active concern with emerging guidelines to improve accuracy and reproducibility (Hall *et al* 2013, Ferraioli *et al* 2018). Also, the best estimates of human vesicle's triglyceride viscosity, and the ratio of the real/imaginary parts of the liver shear modulus under increasingly fibrotic states are uncertain at this time. These can

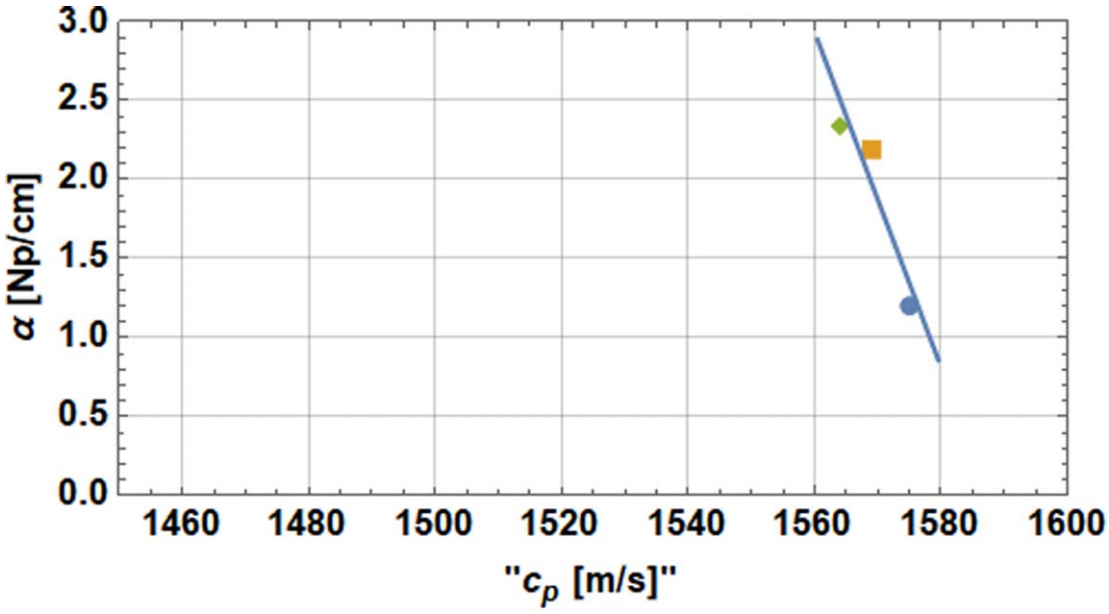


**Figure 5.** Ultrasound attenuation versus speed of sound measurements of steatotic rabbit livers reported by Ghoshal *et al* (2012) at a center frequency near 15 MHz. Data points are group averages for normal (blue dot, $V = 0.015$); intermediate steatotic group (orange square, $V = 0.056$) and steatotic group (green diamond, $V = 0.14$). The blue line represents the application of the composite model with bulk modulus above 2 GPa for the liver and oil components. The solid line in ascending (upward) direction has the volume fraction $V$ beginning at 0% and increasing to 15% at the top.

be refined by careful studies that measure both the shear wave properties and the chemical composition of livers under different states. In particular, extraction and quantification of triglyceride properties from the vacuoles may provide improved estimates of the inherent viscosity term to be used in equation (4). Similarly, the loss component of normal livers, exclusive of any fat, can be estimated from previous studies, however as a liver becomes fibrotic the loss tangent (exclusive of fat accumulation) may change, altering the relationship or proportionality of $G_1$ to $G_{1,\text{im}}$ in the equations within appendix A. These refined estimates should improve the performance of the model under a wider range of pathological conditions.

Other measures can fit within our framework. For example dispersion estimates are linked by physics to the attenuation losses within any causal medium and have been used to measure tissues (Parker *et al* 2015, Ormachea and Parker 2020). Other magnetic resonance imaging and optical imaging systems can be employed, as long as an estimate of both real and imaginary parts of the shear modulus can be obtained and entered into the model.

Our framework can be extended to a calculation of fat volume $V$ based on measurements of the *acoustic* speed of sound and attenuation measured at megahertz frequencies as well. Different forms of mixture or composite models can describe changes in speed of sound and attenuation and have been used in the past (Apfel 1986, Sehgal *et al* 1986, Imbault *et al* 2017, Imbault *et al* 2018, Mast 2000). In our framework, we assume the Christensen composite model still applies as it is based on general principles (Lakes 1999a) and in the equations for compression waves, bulk modulus $B$ replaces shear modulus $G$. Christensen's equations for bulk modulus of a composite material are summarized in appendix B, for the case of spherical inclusions. Thus, one can proceed by measuring the ultrasound speed of sound and attenuation of the tissue, then applying equations (5) and (6) where $G$ is replaced by bulk modulus $B$ for compression waves. Then, the real and imaginary parts of wavenumber are compared with the composite model, producing two equations in two unknowns ($B$ of the liver and $V$ of the fat volume fraction) which can be solved numerically or by nomogram.

As an example, we examine the ultrasound speed of sound and attenuation measured by Ghoshal *et al* (2012) in a steatotic rabbit liver model using broadband ultrasound with a center frequency near 15 MHz. Normal values and two progressively increased fat levels are plotted as data points in figure 5 representing group average values. Also shown is the theoretical model from fat $V = 0$ (bottom of solid line) to $V = 0.15$ (top of solid line). The model assumes that normal liver has a bulk modulus of:

$$B_{\text{liver}} = (2.5 \times 10^9) + (i7.2 \times 10^6), \text{ and}$$
$$B_{\text{fat}} = (2.14 \times 10^9) + (i9 \times 10^7). \tag{11}$$

The real part of these are consistent with the compressibility of water (Kinsler 1982), above 2 GPa, and the imaginary parts are consistent with the attenuation of liver (Mast 2000, Ghoshal *et al* 2012) and common edible

oils (Chanamai and McClements 1998), respectively. At 15 MHz, the attenuation using these parameters would be 0.86 Np $cm^{-1}$ and 12 Np $cm^{-1}$ for normal (fat-free) liver and liquid oil, respectively. The oil attenuation is higher than the values reported by Chanamai and McClements, but this could be due to temperature differences, and the effects of scattering and mode conversion by steatotic vacuoles, which are not explicitly accounted for in the composite model.

However, a comparative disadvantage is present in the case of these ultrasound parameters; as the change in normal liver's speed of sound with increasing amounts of steatosis is a small percent compared to baseline (Mast 2000, Pirmoazen *et al* 2020). Thus, high precision in the measurements will be required, along with careful disentangling of any cofactors that also influence speed of sound and attenuation of the liver.

## 6. Conclusion

By careful examination of the biophysics of composite materials, and the real and imaginary parts of the wave equations, it is possible to reduce a system of equations that models waves in the steatotic liver. The reduced set of equations is comprised of two equations (real and imaginary) in two unknowns (fat volume fraction $V$ and liver modulus $G$ or $B$). Given accurate measurements of attenuation and wave speed as inputs to the system of equations, the volume fraction and modulus can be estimated. Assumptions about the inherent material properties of fat in the liver must be refined by careful independent measurements, and the accuracy of input measurements will require improvements in order to narrow the remaining uncertainties. Ultimately, this approach has the potential to lead to simple and rapid noninvasive assessment of steatosis in clinical examinations.

## Acknowledgments

This work was supported by the Hajim School of Engineering and Applied Sciences and the Department of Electrical and Computer Engineering at the University of Rochester.

## Appendix A

Using Christensen's theory of composite media with inhomogeneous spherical inclusions (Christensen 1969), and assuming a nearly incompressible limit, we can rewrite equation (2) for the explicit case where the liver shear modulus (exclusive of any fat vacuoles) has a real part $G_1$ and an imaginary part $G_{1,\mathrm{im}}$

$$G_{\mathrm{comp}}(\omega) = (G_1 + iG_{1,\mathrm{im}}) + \frac{5(G_1 + iG_{1,\mathrm{im}})[-(G_1 + iG_{1,\mathrm{im}}) + i\boldsymbol{G}_2]V}{3(G_1 + iG_{1,\mathrm{im}}) + 2i\boldsymbol{G}_2}, \tag{A1}$$

where $\boldsymbol{G}_2$ represents the magnitude of the viscous fat term, equation (4). Now, separating out the real and imaginary parts of this equation we have:

$$\mathrm{Re}\,[G_{\mathrm{comp}}(\omega)] = G_1 - \frac{5G_1[3(G_1^2 + G_{1,\mathrm{im}}^2) + 4G_{1,\mathrm{im}}\boldsymbol{G}_2 - 2\boldsymbol{G}_2^2]V}{9G_1^2 + (3G_{1,\mathrm{im}} + 2\boldsymbol{G}_2)^2} \tag{A2}$$

for the real, and then for the imaginary part:

$$\mathrm{Im}[G_{\mathrm{comp}}(\omega)] = G_{1,\mathrm{im}} + \frac{5[-3G_{1,\mathrm{im}}(G_1^2 + G_{1,\mathrm{im}}^2) + 5(G_1^2 + G_{1,\mathrm{im}}^2)\boldsymbol{G}_2 + 2G_{1,\mathrm{im}}\boldsymbol{G}_2^2]V}{9G_1^2 + (3G_{1,\mathrm{im}} + 2\boldsymbol{G}_2)^2}. \tag{A3}$$

As a check, in the limit as $G_{1,\mathrm{im}}$ goes to zero, these equations revert back to the simpler form of equation (8).

The introduction of $G_{1,\mathrm{im}}$ accounts for the lossy behavior of normal, lean liver tissue commensurate with viscoelastic material. However, this represents a third unknown unless set to an *a priori* value, from experimental results and rheological models. Based on our studies and others (Parker *et al* 2019, Ormachea and Parker 2020) we have employed a simplification where $G_{1,\mathrm{im}}$ is set at a small percent (around 5%) of $G_1$, thus reducing the unknowns in the equations to two: $G_1$ and $V$.

## Appendix B

Again applying Christensen's theory of composite media with inhomogeneous spherical inclusions (Christensen 1969), equation (A3) for effective bulk modulus, and assuming a nearly incompressible limit such that the Poisson's ratio of the surrounding matrix is nearly equal to 0.5, we find that

$$B_{\text{comp}}(\omega) = \left[\frac{B_{\text{liver}}(\omega) \cdot B_{\text{fat}}(\omega)}{B_{\text{fat}}(\omega) + (B_{\text{liver}}(\omega) - B_{\text{fat}}(\omega))V}\right], \tag{B1}$$

where $B_{\text{liver}}$ represents the bulk modulus of the fat-free liver, $B_{\text{fat}}$ is the bulk modulus of the fat vacuoles, $B_{\text{comp}}$ is the resulting composite medium effective macroscopic bulk modulus, and $\omega$ is the radial frequency of the waves.

## ORCID iDs

K J Parker https://orcid.org/0000-0002-6313-6605
J Ormachea https://orcid.org/0000-0003-2481-8133

## References

Apfel R E 1986 Prediction of tissue composition from ultrasonic measurements and mixture rules *J. Acoust. Soc. Am.* **79** 148–52
Barr R G *et al* 2015 Elastography assessment of liver fibrosis: society of radiologists in ultrasound consensus conference statement *Radiology* **276** 845–61
Blackstock D T 2000 *Fundamentals of Physical Acoustics* (New York: Wiley) ch 9
Carstensen E L and Parker K J 2014 Physical models of tissue in shear fields *Ultrasound Med. Biol.* **40** 655–74
Chanamai R and McClements D J 1998 Ultrasonic attenuation of edible oils *J. Am. Oil Chem. Soc.* **75** 1447–8
Christensen R M 1969 Viscoelastic properties of heterogeneous media *J. Mech. Phys. Solids* **17** 23–41
Cowin G J, Jonsson J R, Bauer J D, Ash S, Ali A, Osland E J, Purdie D M, Clouston A D, Powell E E and Galloway G J 2008 Magnetic resonance imaging and spectroscopy for monitoring liver steatosis *J. Magn. Reson. Imaging* **28** 937–45
Ferraioli G 2019 Non-invasive assessment of liver steatosis *Ultrasound Med. Biol.* **45** S32–3
Ferraioli G *et al* 2019 Detection of liver steatosis with a novel ultrasound-based technique: a pilot study using mri-derived proton density fat fraction as the gold standard *Clin. Transl. Gastroenterol.* **10** e00081
Ferraioli G, Wong V W, Castera L, Berzigotti A, Sporea I, Dietrich C F, Choi B I, Wilson S R, Kudo M and Barr R G 2018 Liver ultrasound elastography: an update to the WFUMB guidelines and recommendations *Ultrasound Med. Biol.* **44** 2419–40
Fung Y C 1981 *Biomechanics: Mechanical Properties of Living Tissues* (Berlin: Springer)
Ghoshal G, Lavarello R J, Kemmerer J P, Miller R J and Oelze M L 2012 *Ex vivo* study of quantitative ultrasound parameters in fatty rabbit livers *Ultrasound Med. Biol.* **38** 2238–48
Hall T J *et al* 2013 RSNA/QIBA: shear wave speed as a biomarker for liver fibrosis staging *IEEE Int. Ultrasonics Symp. (IUS)* vol 60 (Picastaway, NJ: IEEE) pp 397–400
Imbault M *et al* 2018 Ultrasonic fat fraction quantification using *in vivo* adaptive sound speed estimation *Phys. Med. Biol.* **63** 215013
Imbault M, Faccinetto A, Osmanski B F, Tissier A, Deffieux T, Gennisson J L, Vilgrain V and Tanter M 2017 Robust sound speed estimation for ultrasound-based hepatic steatosis assessment *Phys. Med. Biol.* **62** 3582–98
Jesper D, Klett D, Schellhaas B, Pfeifer L, Leppkes M, Waldner M, Neurath M F and Strobel D 2020 Ultrasound-based attenuation imaging for the non-invasive quantification of liver Fat - A pilot study on feasibility and inter-observer variability *IEEE J. Transl. Eng. Health Med.* **8** 1–9
Kinsler L E 1982 *Fundamentals of Acoustics, Appendix A10* (New York: Wiley)
Kramer H, Pickhardt P J, Kliewer M A, Hernando D, Chen G H, Zagzebski J A and Reeder S B 2017 Accuracy of liver fat quantification with advanced CT, MRI, and ultrasound techniques: prospective comparison With MR spectroscopy *Am. J. Roentgenol.* **208** 92–100
Lakes R S 1999a *Viscoelastic Solids* (Boca Raton, FL: CRC Press)
Lakes R S 1999b *Viscoelastic Solids* (Boca Raton, FL: CRC Press) ch 9
Lee S S and Park S H 2014 Radiologic evaluation of nonalcoholic fatty liver disease *World J. Gastroenterol.* **20** 7392–402
Lin Y-H, Wan Y-L, Tai D-I, Tseng J-H, Wang C-Y, Tsai Y-W, Lin Y-R, Chang T-Y and Tsui P-H 2019 Considerations of ultrasound scanning approaches in non-alcoholic fatty liver disease assessment through acoustic structure quantification *Ultrasound Med. Biol.* **45** 1955–69
Mast T D 2000 Empirical relationships between acoustic parameters in human soft tissues *Acoust. Res. Lett. Online* **1** 37–42
Nasr P, Fredrikson M, Ekstedt M and Kechagias S 2020 The amount of liver fat predicts mortality and development of type 2 diabetes in non-alcoholic fatty liver disease *Liver Int.* **40** 1069–78
Nguyen T N, Podkowa A S, Tam A Y, Arnold E C, Miller R J, Park T H, Do M N and Oelze M L 2019 Characterizing fatty liver *in vivo* in rabbits, using quantitative ultrasound *Ultrasound Med. Biol.* **45** 2049–62
Öner M and Kocakoç I D 2017 JMASM 49: a compilation of some popular goodness of fit tests for normal distribution: Their algorithms and MATLAB codes (MATLAB) *J. Mod. Appl. Stat. Methods* **16** 547–75
Ormachea J and Parker K J 2020 Comprehensive viscoelastic characterization of tissues and the inter-relationship of shear wave (group and phase) velocity, attenuation and dispersion *Ultrasound Med. Biol.* **46** 3448–59
Parker K J 2014 A microchannel flow model for soft tissue elasticity *Phys. Med. Biol.* **59** 4443–57
Parker K J 2015 Experimental evaluations of the microchannel flow model *Phys. Med. Biol.* **60** 4227–42
Parker K J, Ormachea J, Drage M G, Kim H and Hah Z 2018a The biomechanics of simple steatosis and steatohepatitis *Phys. Med. Biol.* **63** 105013
Parker K J, Ormachea J, Will S and Hah Z 2018b Analysis of transient shear wave in lossy media *Ultrasound Med. Biol.* **44** 1504–15
Parker K J, Partin A and Rubens D J 2015 What do we know about shear wave dispersion in normal and steatotic livers? *Ultrasound Med. Biol.* **41** 1481–7
Parker K J, Szabo T and Holm S 2019 Towards a consensus on rheological models for elastography in soft tissues *Phys. Med. Biol.* **64** 215012
Pirmoazen A M, Khurana A, El Kaffas A and Kamaya A 2020 Quantitative ultrasound approaches for diagnosis and monitoring hepatic steatosis in nonalcoholic fatty liver disease *Theranostics* **10** 4277–89
Poul S S and Parker K J 2021 Fat and fibrosis as confounding cofactors in viscoelastic measurements of the liver *Phys. Med. Biol.* **66** 045024
Romero-Gómez M and Cortez-Pinto H 2017 Detecting liver fat from viscoelasticity: How good is CAP in clinical practice? The need for universal cut-offs *J. Hepatol.* **66** 886–7

Sehgal C M, Brown G M, Bahn R C and Greenleaf J F 1986 Measurement and use of acoustic nonlinearity and sound speed to estimate composition of excised livers *Ultrasound Med. Biol.* **12** 865–74

Sharma A K, Reis J, Oppenheimer D C, Rubens D J, Ormachea J, Hah Z and Parker K J 2019 Attenuation of shear waves in normal and steatotic livers *Ultrasound Med. Biol.* **45** 895–901

Starekova J and Reeder S B 2020 Liver fat quantification: where do we stand? *Abdom. Radiol.* **45** 3386–99

Tamura K, Mamou J, Yoshida K, Hachiya H and Yamaguchi T 2020 Ultrasound-based lipid content quantification using double-Nakagami distribution model in rat liver steatosis *Jpn. J. Appl. Phys.* **59** SKKE23

Xia M F, Yan H M, He W Y, Li X M, Li C L, Yao X Z, Li R K, Zeng M S and Gao X 2012 Standardized ultrasound hepatic/renal ratio and hepatic attenuation rate to quantify liver fat content: an improvement method *Obesity* **20** 444–52

Younossi Z M, Koenig A B, Abdelatif D, Fazel Y, Henry L and Wymer M 2016 Global epidemiology of nonalcoholic fatty liver disease-Meta-analytic assessment of prevalence, incidence, and outcomes *Hepatology* **64** 73–84

Zhang M, Castaneda B, Wu Z, Nigwekar P, Joseph J V, Rubens D J and Parker K J 2007 Congruence of imaging estimators and mechanical measurements of viscoelastic properties of soft tissues *Ultrasound Med. Biol.* **33** 1617–31

Zhang Y N, Fowler K J, Hamilton G, Cui J Y, Sy E Z, Balanay M, Hooker J C, Szeverenyi N and Sirlin C B 2018 Liver fat imaging-a clinical overview of ultrasound, CT, and MR imaging *Br. J. Radiol.* **91** 20170959